ROLE OF INITIAL CONDITIONS IN THE EVOLUTION OF AN AXISYMMETRIC TURBULENT JET DUE TO GEOMETRICAL EFFECTS ON THE NEAR-FIELD COHERENCE

Massimiliano Breda
Department of Aeronautics
Imperial College
South Kensington Campus, London, SW7 2AZ
mb2014@ic.ac.uk

Oliver R. H. Buxton
Department of Aeronautics
Imperial College
South Kensington Campus, London, SW7 2AZ
o.buxton@imperial.ac.uk

ABSTRACT

In this paper the role of initial conditions in affecting the evolution of an axisymmetric turbulent jet is examined. The jet's near-field large-scale coherent structures (the so called Kelvin-Helmholtz vortex rings) are manipulated with the aid of non-circular exit geometries of identical open area D_e^2. Hot-wire anemometry and 2D-2C planar PIV were completed between the exit of the jet and 26 D_e downstream, to study the effect of round, square and fractal geometries on the coherent structures and on the jet's evolution both spatially and temporally. It is found the fractal geometry breaks up the jet's coherent structures leading to a delay of the overall jet development, meaning some of the jet properties can be rescaled in terms of eddy turnover times. Moreover, non-equilibrium dissipation is found for all jets at issue, indicating it takes place for this shear flow independently of the initial conditions. This property is common to axisymmetric wakes and grid-generated flows too.

INTRODUCTION

Recent studies have been focused on understanding how the initial conditions of a shear flow affect its evolution towards the self-similar state. Since the work of Townsend (1976), it has been generally accepted that across its evolution a shear flow would become asymptotically independent of the initial conditions. This was backed by the work of Antonia & Zhao (2001), who found that a "top-hat" and a fully developed axisymmetric round pipe jet would become self-similar after the same streamwise distance. However, George (1989) argued that the self-similar state would be linked to the coherent structures. The work of Antonia & Pearson (2000) hinted in this direction since the authors found that different axisymmetric wake generators had different mean energy dissipation rates. In the present study, the role of the initial conditions on the evolution of an axisymmetric turbulent jet is studied further by manipulating the coherent structures of an axisymmetric jet with the aid of noncircular exit geometries.

The latter have been shown to significantly affect the near-field state of an axisymmetric jet. Gutmark *et al.* (1989), investigating triangular, square and elliptical jets, showed that a combination of corners and flat sides combined the small scale turbulence generated at the corners with the coherent structures at the flat sides. Shakouchi & Iriyama (2013) showed that a large wetted perimeter led to an increased mixing between the turbulent jet and the irrotational free stream. Therefore in order to further explore the effect of the exit geometry on the coherent structures, a square and fractal orifice are compared to a round one. The latter fractal geometry has been previously studied on the perimeter of axisymmetric wake generators where a breakup of the coherent structures and a reduction of the shedding energy were observed (Nedić *et al.*, 2015). Having shown the reduction in energy content of the coherent structures, Nedić *et al.* (2013*b*) examined the self-similar region of the flow and found novel scaling exponents for the spatial evolution of the wake's width and centreline velocity decay. This was attributed to the presence of non-equilibrium (NE) dissipation (refer to Vassilicos (2015) for a complete description of the topic), where the inter-scale energy transfer is not instantaneously in equilibrium with the turbulent kinetic energy dissipation rate. When non-equilibrium dissipation is present, the dissipation coefficient C_ε is not constant but a function of local Reynold number Re_{λ_f} (eq. (1)) and of the global one Re_G (eq. (4)), as shown in eq. (2).

$$Re_{\lambda_f} = \frac{\lambda_f u'}{\nu} \tag{1}$$

$$\begin{aligned} C_\varepsilon \equiv \frac{\varepsilon \mathscr{L}}{u'^3} \sim \frac{Re_G^{1/2}}{Re_{\lambda_f}} \neq \text{constant} \\ \forall Re_{\lambda_f} = Re_{\lambda_f}(x) \neq \text{constant} \end{aligned} \tag{2}$$

Here, ε is the dissipation, u' the root-mean-square (r.m.s.) of the streamwise velocity fluctuations and $\mathscr{L}$ the integral length scale. In order to study how the exit geometry affects the near-field coherent structures and the subsequent jet's evolution, two dimensional-two component (2D-2C) planar particle image velocimetry (PIV) and hot-wire constant temperature anemometry (CTA) are performed.

METHODOLOGY

The study is conducted in a newly designed jet facility at Imperial College London. The flow is conditioned with a honeycomb and two screens of decreasing mesh size, before it enters a 5$^{\text{th}}$ order polynomial contraction. Preliminary testing showed the exit flow had a sharp "top-hat" mean velocity profile. Three different orifices of thickness 0.1 mm and of identical open area (D_e^2), as shown in fig. 1, are attached to the nozzle. Apart from the jet exit shape, all the conditions of the jets are kept the same. Three Reynolds numbers of $Re_G = 3,000$ ($U_e = 2.98\,\text{m/s}$), $Re_G = 10,000$ ($U_e = 9.93\,\text{m/s}$) and $Re_G = 31,000$ ($U_e = 30.80\,\text{m/s}$) were chosen, where two different regimes of Kelvin-Helmholtz vortices were expected in order to test the Re_G-dependence.

The flow is studied between 0 and $26D_e$ with two-dimensional two-component (2D-2C) planar PIV, with the laser sheet placed across the centreline of the jets. A seeded low speed co-flow (speed of $\approx 0.1\,\text{m/s}$) was added to avoid biasing the experiments as background fluid is entrained into the jet. In total, 1,500 images were acquired per jet configuration at various streamwise locations. The fields of view were $9D_e \times 6.7D_e$. An initial interrogation area of 64×64 pixels was used to process the images recursively with a final window size of 16×16 pixels. A 50 % overlap between adjacent interrogation areas was used leading to a final vector spacing of $0.03D_e$. Following the preliminary results, highly resolved planar 2D2C PIV to investigate the velocity gradients was performed in the near and far-field (23-26 D_e, where the Reynolds stresses become self-similar). This time, a final interrogation area of 12x12 pixels with 50 % overlap was used. This led to a vector spacing of 0.013 D_e and a spatial resolution between 3 and 4 Kolmogorov length scales (η) and ranged between 0.08-0.12 longitudinal Taylor length scales (λ_f). The testing campaign was concluded with single hot-wire constant temperature anemometry (CTA) in the near- and far-field at $Re_G = 10,000$ and $Re_G = 31,000$, with a sampling rate of 100 kHz, which was subsequently low-pass filtered at 30 kHz. Gold-plated 55P01 Dantec hot wires were used, the ratio between wire length and diameter was 250 (wire diameter $5\,\mu$m, spatial resolution $1.25\,\text{mm} \approx 10\eta$), the overheat ratio was set at 0.8 and the square wave response was above 40 kHz.

$$D_e = \sqrt{\text{Exit area}} \qquad U_e = \frac{\text{Volumetric flow rate}}{\text{Exit area}} \tag{3}$$

$$Re_G = \frac{U_e D_e}{\nu} \tag{4}$$

RESULTS

In order to understand how the exit geometry affects the large scale coherent structures (the Kelvin-Helmholtz vortex rings), the two-point spatial correlation R_{vx} of the radial velocity component v in the streamwise direction x was calculated as a function of the stremawise increment ξ across the jet shear layer (defined as the peak of streamwise fluctuations), where the coherent structures reside in the near-field, as shown in eq. (6). The ensemble average $\langle * \rangle$ indicates an average in both time and space (within a 3×3 vector box surrounding location (x,r) to improve the statistical convergence).

$$V = \overline{v} + v' \tag{5}$$

$$R_{vx}(x,r,\xi) = \frac{\langle v'(x,r)v'(x+\xi,r)\rangle}{\langle v'^2(x,r)\rangle^{1/2}\langle v'^2(x+\xi,r)\rangle^{1/2}} \tag{6}$$

As shown in fig. 2a, the fractal geometry suppresses the anti-correlation of R_{vx}, which is usually associated with the vorticity of the Kelvin-Helmholtz vortex rings, suggesting they have been broken-up. This may be seen in the PIV images in fig. 3, where the fractal jet shows no signs of large coherent structures. Moreover, the turbulent kinetic energy production region of the fractal jet was found to be extended compared to the round and square jets, as shown in fig. 2b. This indicated that the break up of the coherent structures altered the initial development of the jet, suggesting that the fractal jet development may be delayed further downstream compared to the other two cases. As stated by Hunt (1994), the turbulent structure of a shear flow retains "memory" of the initial conditions, since the eddy convection time is linked to its growing time scale. Hence, despite irrotational fluid being entrained into the jet stream, the initial conditions still affect the development of the eddies through the large-scale structures far downstream. Therefore, the jet physics is revisited in terms of the advection time scale (related to the mean velocity) and the number of eddy turnover times undergone whilst the flow advects a distance x.

$$N_{e_x}(x) = \frac{\text{Advection time}}{\text{Eddy turnover time}} = \int_{1D_e}^{x} \frac{\overline{u'^2}(\xi)^{1/2}}{\mathscr{L}_{ux}(\xi)\overline{u}(\xi)} \mathrm{d}\xi. \tag{7}$$

Here, the integration is initiated at $x/D_e = 1$ since neither the velocity fluctuations nor the velocity correlations are well defined at the "top-hat" jet exit. In the near-field, the calculations are performed at the shear layer (found as the peak of r.m.s. velocity fluctuations). From the hot-wire data, the integral length scale $\mathscr{L}_{ux}$ is calculated integrating the autocorrelation of the velocity fluctuations in time delay τ from $\tau = 0$ to $\tau = \mathscr{T}$, where $\mathscr{T} \to \infty$. From a sensitivity analysis, $\mathscr{T} = 20\tau'$ (where τ' is the time delay for the first zero-crossing of the correlation) was found to be sufficient. The autocorrelation in time was converted into space by multiplying by the mean velocity and assuming the Taylor's hypothesis.

$$R(x,\tau) = \frac{u'(x,t)u'(x,t+\tau)}{u'^2(x)} \tag{8}$$

$$\mathscr{L}_{ux}(x) = \overline{u}(x) \int_0^{\mathscr{T}} R(x,\tau)\ \mathrm{d}\tau \tag{9}$$

Now the jet properties are revisited in terms of N_{e_x}, to find out which ones are unique and which ones are simply delayed by the break-up of the coherent structures.

First the entrainment rate of background fluid into the turbulent jet is considered. Manipulating the near-field coherent structures has been shown to significantly affect the entrainment rate and mixing of irrotational flow into the jet's turbulent stream (Brown & Roshko, 1974) and as a consequence its evolution towards the self-similar state. Here, the entrainment rate is evaluated in terms of the local spatial gradient of the volume flux Q in the streamwise direction x, defined in Craske & van Reeuwijk (2014) as a function of the entrainment parameter α, the characteristic jet velocity u_m and the characteristic jet width r_m. The entrainment parameter α contains contributions from the turbulent kinetic energy production and from the energy, momentum and volume fluxes. It is also consistent with the entrainment model of Kaminski *et al.* (2005).

$$\frac{\partial Q}{\partial x} = 2\alpha r_m u_m. \tag{10}$$

Due to the finite size of the field of view, the integration of the terms in table 1 is done up to the radial location R_0 where the inwards radial velocity v is 1% of the streamwise centreline velocity u_{cl}.

$$\overline{v}(x,R_0) = 0.01 u_{cl}(x) \tag{11}$$

Table 1: Terms of the entrainment parameter equation

Term	Equation
Volume Flux	$Q = 2\int_0^{R_0} \overline{u} r dr$
Momentum Flux	$M = 2\int_0^{R_0} \overline{u}^2 r dr$
Characteristic jet width	$r_m = \frac{Q}{M^{1/2}}$
Characteristic jet velocity	$u_m = \frac{M}{Q}$
Turbulence Production	$\delta_m = \frac{4}{u_m^3 r_m}\int_0^{R_0} \overline{u'v'}\frac{\partial \overline{u}}{\partial r} r dr$
Energy Flux	$\gamma_m = \frac{4}{u_m^3 r_m^2}\int_0^{R_0} \overline{u}^3 r dr$
Entrainment parameter	$\alpha = -\frac{\delta_m}{2\gamma_m} + \frac{Q}{2M^{1/2}}\frac{\partial}{\partial x}(\ln \gamma_m)$

It is shown that the fractal geometry leads to a reduction of the entrainment parameter α, however when $\partial Q/\partial x$ is evaluated in terms of eddy turnover times, all jets tend asymptotically to the same trend after approximately 3 N_{e_x}, as shown in fig. 4. Hence, it is found that despite the different exit geometries, all jets have a comparable entrainment rate when rescaled accordingly after an initial "transient" geometry-specific period of 3-4 large-scale eddy turnovers. In terms of mixing, at $Re_G = 3{,}000$ the round jet has the highest spreading rate, while the fractal jet the lowest. At $Re_G = 10{,}000$, all jets have a comparable spreading rate, however due to the different location of the virtual origin (assuming the jet evolves from a single point source of momentum), the round jet is always the widest in the far-field while the fractal jet the narrowest.

The jet physics are evaluated further by looking at the terms of the time averaged momentum equation (TAME), split into radial (eq. (12)) and streamwise (eq. (13)) directions as in Chao & Sandborn (1966).

$$\begin{aligned}\overline{v}\frac{\partial \overline{v}}{\partial r} + \overline{u}\frac{\partial \overline{v}}{\partial x} + \frac{\partial \overline{v'^2}}{\partial r} + \frac{1}{r}(\overline{v'^2} - \overline{w'^2}) + \frac{\partial \overline{u'v'}}{\partial x} = \\ -\frac{1}{\rho}\frac{\partial p}{\partial r} + \nu\left(\frac{\partial^2 \overline{v}}{\partial r^2} + \frac{1}{r}\frac{\partial \overline{v}}{\partial r} - \frac{\overline{v}^2}{r^2} + \frac{\partial^2 \overline{v}}{\partial x^2}\right)\end{aligned} \tag{12}$$

$$\begin{aligned}\overline{v}\frac{\partial \overline{u}}{\partial r} + \overline{u}\frac{\partial \overline{u}}{\partial x} + \frac{\partial \overline{u'v'}}{\partial r} + \frac{\overline{u'v'}}{r} + \frac{\partial \overline{u'^2}}{\partial x} = \\ -\frac{1}{\rho}\frac{\partial p}{\partial x} + \nu\left(\frac{\partial^2 \overline{u}}{\partial r^2} + \frac{1}{r}\frac{\partial \overline{u}}{\partial r} + \frac{\partial^2 \overline{u}}{\partial x^2}\right)\end{aligned} \tag{13}$$

The data are taken in the same region $2-5D_e$, however they are plotted in terms of eddy turnover time. Note that the terms containing the pressure gradients and the out-of-plane fluctuations w' could not be computed directly from the data, and were thus derived from the residual of the balance of the various terms. Overall the terms that remain significant throughout the jet's evolution are the pressure terms, the streamwise mean velocity gradient, the Reynolds shear stress and its gradient. It is found that the radially evolving terms of the mean momentum follow the same trend after 3-4 N_{e_x}, as shown in fig. 5b, since the noncircular jets are evolving towards an axisymmetric state. Similar findings had been seen by Nedić *et al.* (2013*a*), which showed axisymmetric wakes generated by both square and fractal plates would quickly return to axisymmetry after an initial development region. However, the jets show different trends for the streamwise mean momentum terms, as shown in fig. 5a, indicating the forcing through a noncircular geometry has a larger effect on the evolution of the streamwise mean flow. The influence of the fluctuating velocity is found to be minor compared to the mean flow. Hence, both the TAME and the entrainment rate indicates that the jets have an initial development region, which lasts between 3-4 N_{e_x}, where the jet evolves towards an axisymmetric state. After this distance, all jets evolve in a comparable fashion radially, irrespectively of the jet exit.

Overall, the noncircular forcing is found to significantly affect the properties of the jets only for a small "developing" region near the jet exit. Now, their subsequent evolution towards the self-similar state is examined to evaluate if the argument of Townsend (1976) (the jets become asymptotically independent of the initial conditions) or of George (1989) (the self-similar state is linked to the coherent structures) holds. If it is assumed that classical dissipation holds ($C_\varepsilon \sim$ constant), the self-similar scalings are widely reported in Tennekes & Lumley (1972). A preliminary analysis indicated that even if it was assumed that $C_\varepsilon = C_\varepsilon(x)$, the same scalings for centreline velocity u_{cl} and the jet half-width $r_{1/2}$ would be found due to the constant momentum flux of the jet. This was found to be the case experimentally. Therefore, traces of non-equilibrium dissipation were looked for in the microscales, dissipation and

dissipation coefficient, where the following scalings were expected:

$$\eta \sim x \qquad \varepsilon \sim x^{-4} \qquad C_\varepsilon \sim \text{constant} \tag{14}$$

The region probed was between 24 and 26 D_e downstream. As observed in fig. 6a, $\varepsilon \sim x^\alpha$, where $\alpha \simeq -3$, which is lower than the value predicted by the classical theories. This reflects on the Kolmogorov length scale which scales as $\eta \sim x^{0.8}$. Additionally, calculating C_ε from both the PIV and the CTA data, it is found C_ε is a function of both $Re_G^{1/2}$ and of Re_{λ_f}, as shown in fig. 6b. This behaviour clearly outlines the presence of non-equilibrium dissipation together with classical scalings for centreline velocity and jet half-with. This was also concurrent to self-similar mean velocity and locally self-similar fluctuating Reynolds stresses profiles (i.e. normalised by a local value of the Reynolds stress rather than of the centreline velocity). Comparable findings were found by Dairay *et al.* (2015) for axisymmetric wakes, indicating it is not a unique behaviour of axisymmetric jets, even though for that shear flow the presence of non-equilibrium dissipation was marked by novel scaling exponents for the wake width and velocity deficit (Nedić *et al.*, 2013*b*). This is the first time traces of non-equilibrium dissipation have been found for an axisymmetric jet. Moreover, this type of dissipation appeared for all jets at issue, independently of the state of the coherent structures and of the initial conditions. This indicates that the coherent structures can affect the rate at which the jet develops, however the mechanics far away from the jet exits remains unaffected by them. It is noted, Hearst & Lavoie (2014) testing fractal grid generated flows showed that initially the flow would have non-equilibrium dissipation but then it transitioned to the classical $C_\varepsilon \sim$ constant. Since the classical dissipation law has been documented for axisymmetric jets too, they may eventually transition to the classical state, however this distance was not reached in the present experiment.

CONCLUSIONS

This study has analysed the role of the initial conditions in affecting the evolution of an axisymmetric turbulent jet towards its self-similar state. Noncircular geometries were used to manipulate the near-field coherent structures and the spatial and temporal properties of the jets were measured with planar PIV and hot-wire anemometry. The fractal geometry is found to break-up the jet coherent structures, causing a delay of the overall jet development further away from the jet's exit. In fact, once the properties are re-scaled in terms of eddy turnover times, the terms involving the radial evolution and entrainment are found to be comparable between the jets irrespective of the initial conditions. The noncircular forcing is found, however, to affect the streamwise evolution of the mean momentum since the streamwise terms of the TAME do not collapse in the region studied. Looking at the jet evolution of the self-similar state, the jets are found to have the same scaling exponents for centreline velocity and jet half-width as predicted by the classical theories. However, at the microscales, non-equilibrium dissipation is found, as shown by the new scaling exponents of dissipation and of the Kolmogorov length scale η. Moreover, this is found concurrent to locally self-similar profiles of the Reynolds stresses. Such properties are common to all jets studied, suggesting, that despite the very different initial conditions, the evolution downstream of the jets is unaffected by the state of the coherent structures.

REFERENCES

Antonia, R. A. & Pearson, B. 2000 Effect of initial conditions on the mean energy dissipation rate and the scaling exponent. *Physical Review E* **62** (6), 8086–8090.

Antonia, R. A. & Zhao, Q. 2001 Effect of initial conditions on a circular jet. *Experiments in Fluids* **31** (3), 319–323.

Brown, Garry L. & Roshko, Anatol 1974 On density effects and large structure in turbulent mixing layers. *Journal of Fluid Mechanics* **64**, 775–816.

Chao, J. L. & Sandborn, V. A. 1966 Evaluation of the momentum equation for a turbulent wall jet. *Journal of Fluid Mechanics* **26**, 819–828.

Craske, John & van Reeuwijk, Maarten 2014 Energy dispersion in turbulent jets. Part 1: Direct simulation of steady and unsteady jets. *Journal of Fluid Mechanics* **763**, 500–537.

Dairay, Thibault, Obligado, Martin & Vassilicos, John Christos 2015 Non-equilibrium scaling laws in axisymmetric turbulent wakes. *Journal of Fluid Mechanics* **781**, 166–195.

George, William K. 1989 The Self-preservation of turbulent flows and its relation to initial conditions and coherent structures. *Tech. Rep.*. University at Buffalo, Buffalo, New York, USA.

Gutmark, Ephraim, Schadow, K. C. & Parr, T 1989 Noncircular jets in combustion systems. *Experiments in Fluids* **7**, 248–258.

Hearst, R. Jason & Lavoie, Philippe 2014 Decay of turbulence generated by a square-fractal-element grid. *Journal of Fluid Mechanics* **741**, 567–584.

Hunt, Julian Charles Roland 1994 Atmospheric jets and plumes. In *Recent Research Advances in the Fluid Mechanics of Turbulent Jets and Plumes* (ed. P. A. Davies & M. J. Valente Neves), pp. 309–334. London: NATO ASI Series.

Kaminski, Edouard, Tait, Stephen & Carazzo, Guillaume 2005 Turbulent entrainment in jets with arbitrary buoyancy. *Journal of Fluid Mechanics* **526**, 361–376.

Nedić, Jovan, Ganapathisubramani, Bharathram & Vassilicos, John Christos 2013*a* Drag and near wake characteristics of flat plates normal to the flow with fractal edge geometries. *Fluid Dynamics Research* **45** (061406).

Nedić, Jovan, Supponen, O., Ganapathisubramani, Bharathram & Vassilicos, John Christos 2015 Geometrical influence on vortex shedding in turbulent axisymmetric wakes. *Physics of Fluids* **27** (035103).

Nedić, Jovan, Vassilicos, John Christos & Ganapathisubramani, Bharathram 2013*b* Axisymmetric turbulent wakes with new nonequilibrium similarity scalings. *Physical Review Letters* **111** (144503).

Shakouchi, Toshihiko & Iriyama, Shota 2013 Flow characteristics of submerged free jet flow from petal-shaped nozzle. In *4th International Conference on Jets, Wakes and Separated Flows*.

Tennekes, Henk & Lumley, John L. 1972 *A First Course in Turbulence*, 1st edn. Cambridge, Massachusetts; London: M.I.T. Press.

Townsend, A. A. 1976 *The Structure of Turbulent Shear Flow*, 2nd edn. New York: Cambridge University Press.

Vassilicos, John Christos 2015 Dissipation in Turbulent Flows. *Annual Review of Fluid Mechanics* **47**, 95–114.

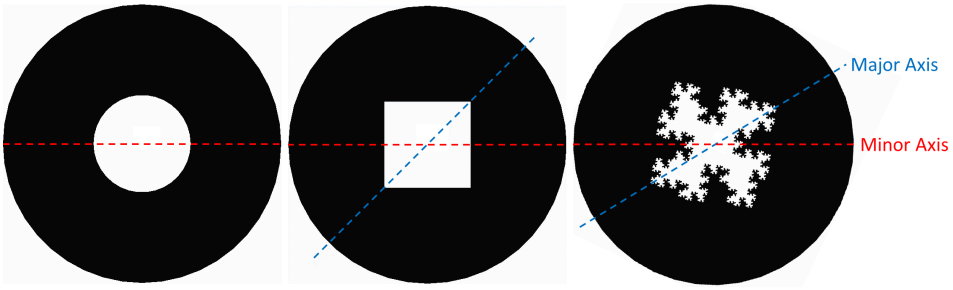

(a) Round (b) Square (c) Fractal

Figure 1: Jet exits

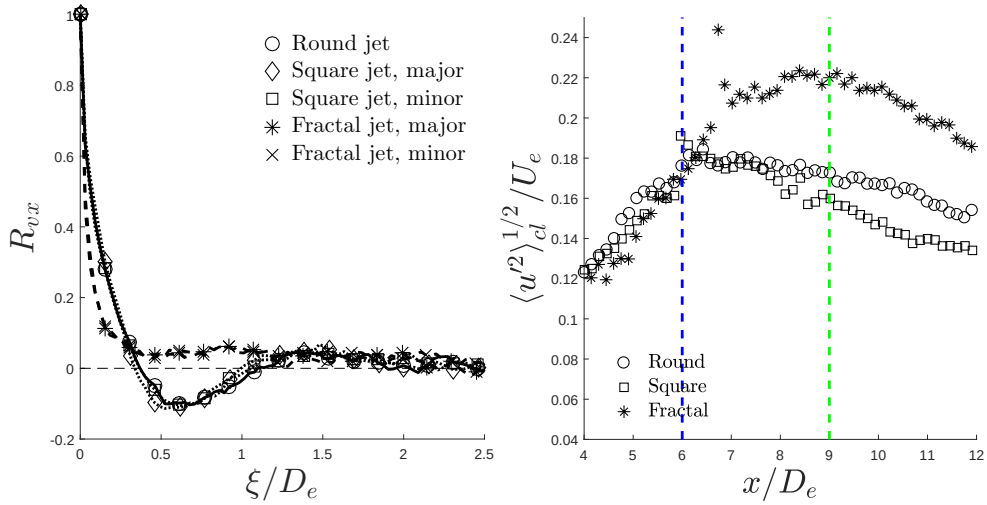

(a) (b)

Figure 2: (a) Two point correlation R_{vx} at 2 D_e at shear layer and (b) Turbulent production region at jet centreline at $Re_G = 10,000$.

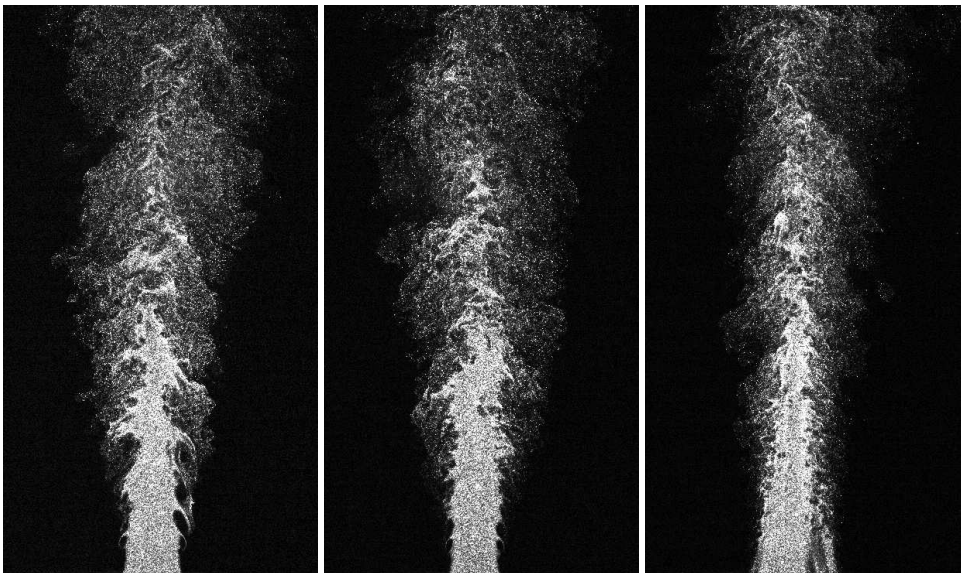

(a) Round (b) Square (c) Fractal

Figure 3: PIV images with co-flow switched off, for visualisation purposes only.

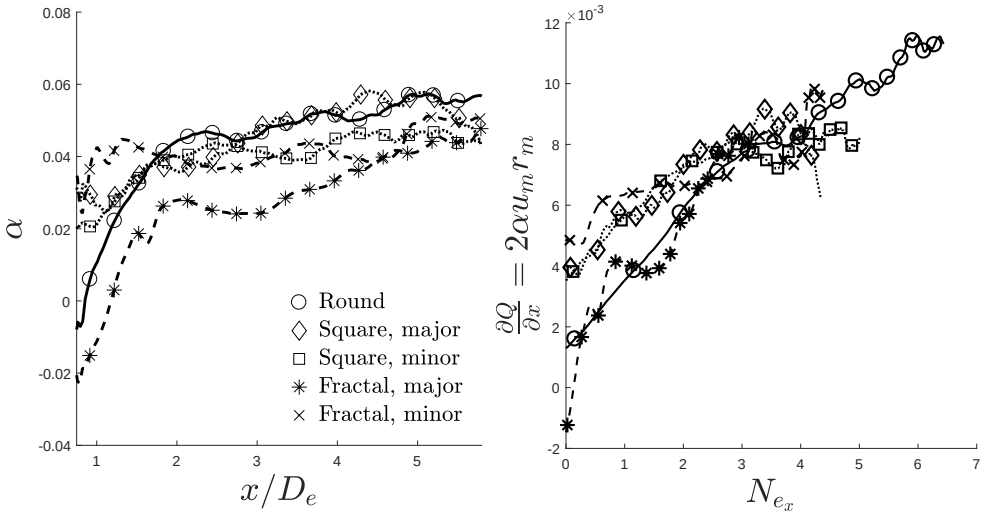

Figure 4: (a) Entrainment parameter and (b) local entrainment rate as a function of N_{e_x} at $Re_G = 10,000$.

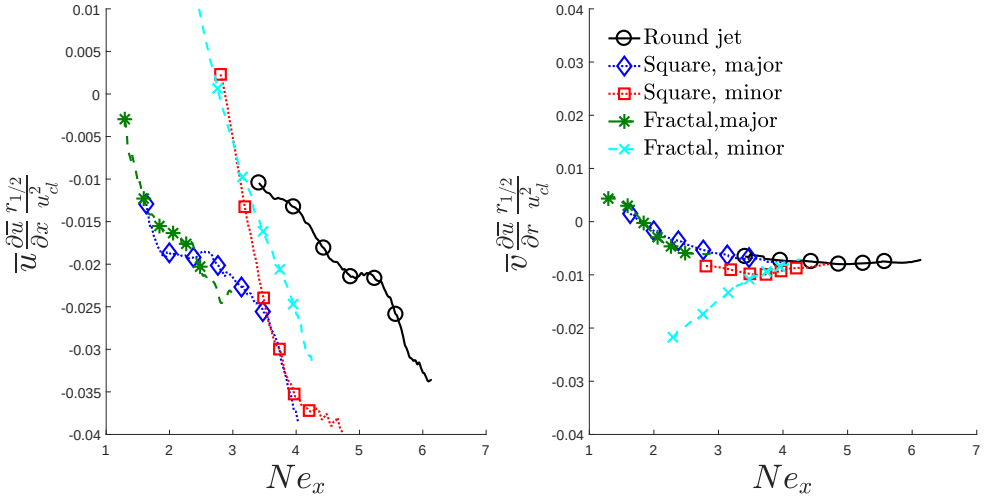

Figure 5: (a) Streamwise and (b) radial terms of the TAME at $Re_G = 10,000$.

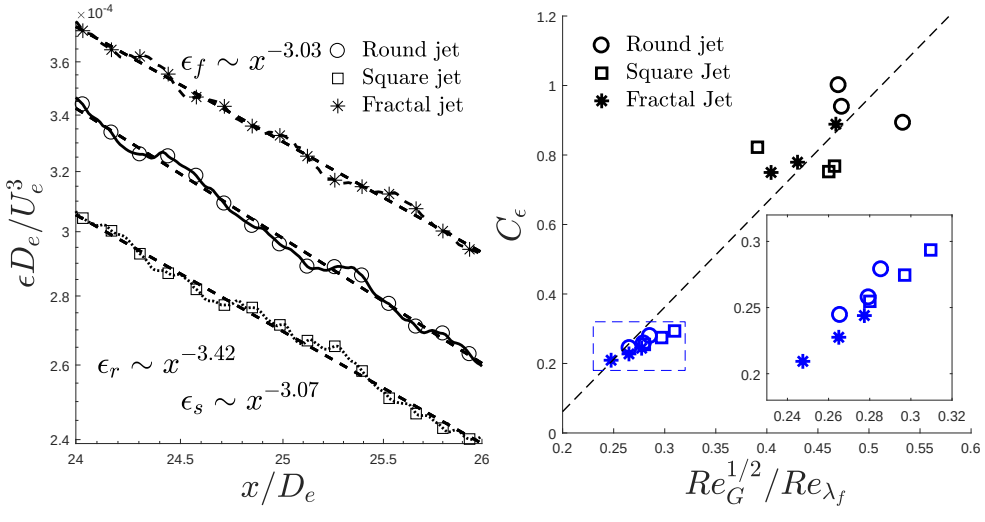

Figure 6: (a) Dissipation rate ε at $Re_G = 10,000$ and (b) dissipation coefficient C_ε at $Re_G = 10,000$ (black) and at $Re_G = 31,000$ (blue).